ELSEVIER

Journal of Atmospheric and Solar-Terrestrial Physics 67 (2005) 1865–1871

Journal of ATMOSPHERIC AND SOLAR-TERRESTRIAL PHYSICS

www.elsevier.com/locate/jastp

Numerical simulations of MHD dynamos

Daniel O. Gómez[a,b,*], Pablo Mininni[b]

[a]*Instituto de Astronomía y Física del Espacio, CC. 67, Suc. 28, 1428 Buenos Aires, Argentina*
[b]*Departamento de Física, Facultad de Ciencias Exactas y Naturales, Universidad de Buenos Aires, 1428 Buenos Aires, Argentina*

Available online 2 November 2005

Abstract

The generation of magnetic fields in space plasmas and in astrophysics is usually described within the framework of magnetohydrodynamics. Turbulent helical flows produce magnetic fields very efficiently, with correlation length scales larger than those characterizing the flow. Within the context of the solar magnetic cycle, a turbulent dynamo is responsible for the so-called *alpha* effect, while the *Omega* effect is associated to the differential rotation of the Sun.

We present direct numerical simulations of turbulent magnetohydrodynamic dynamos including two-fluid effects such as the Hall current. More specifically, we study the evolution of an initially weak and small-scale magnetic field in a system maintained in a stationary regime of hydrodynamic turbulence, and explore the conditions for exponential growth of the magnetic energy. In all the cases considered, we find that the dynamo saturates at the equipartition level between kinetic and magnetic energy, and the total energy reaches a Kolmogorov power spectrum.

Keywords: Magnetohydrodynamics; Magnetic dynamo; Numerical simulations

1. Introduction

Within the framework of magnetohydrodynamics (MHD), dynamo mechanisms involve an efficient conversion of kinetic energy into magnetic energy. The onset of a dynamo can often be studied within the kinematic approximation. During this stage, the velocity field remains unaffected by the relatively weak magnetic field, whose intensity grows exponentially fast. Kinematic dynamos have been intensively studied in recent years and are reasonably well understood (see Childress and Gilbert (1995) for a review). On the other hand, the study of the nonlinear stages leading to the saturation of the dynamo is just beginning, thanks to the advent of fast computers allowing high Reynolds number simulations. The solar cycle has been thoroughly studied within the context of the so-called *alpha-Omega* model. The *Omega* effect corresponds to the enhancement of the toroidal magnetic field, caused by the stretching of (initially poloidal) field lines by the solar differential rotation. On the other hand, the *alpha* effect is required to convert part of the toroidal magnetic field back to poloidal field to maintain the cycle. The role of the *alpha* effect is performed by a small scale and turbulent flow, concentrated in the solar convective region. In this paper we focus on a numerical study of turbulent MHD dynamos, with the main goal of providing some insight toward a microscopic theory of the *alpha* effect.

The relevance of two-fluid effects has been pointed out in several astrophysical problems in recent years (Balbus and Terquem, 2001; Sano and Stone, 2002; Mininni et al., 2002, 2003a). Within the solar-terrestrial environment, two-fluid effects are very important to determine the efficiency of magnetic reconnection at the Earth's magnetopause and magnetotail (Øieroset et al.,

*Corresponding author. Fax: +54 11 47868114.
E-mail addresses: dgomez@df.uba.ar (D.O. Gómez), mininni@df.uba.ar (P. Mininni).
URL: http://astro.df.uba.ar.

1364-6826/$ - see front matter © 2005 Published by Elsevier Ltd.
doi:10.1016/j.jastp.2005.01.016

2001; Deng and Matsumoto, 2001). Simulations of magnetic reconnection including the Hall current, are reported elsewhere (Morales et al., 2004). The standard magnetohydrodynamic framework for the study of astrophysical plasmas may not be adequate in the presence of strong magnetic fields and/or low particle densities. Under these circumstances, Ohm's law should be extended to include two-fluid effects through the Hall and the electron pressure terms.

In the present work, we report results from direct numerical simulations of dynamo action in MHD and Hall-MHD with strong kinetic helical forcing.

The paper is organized in the following fashion. In Section 2 we introduce the theoretical framework and the equations. In Section 3 we give a brief overview of recent results on turbulence and turbulent dynamos. Our numerical results are presented in Section 4. Finally, we list our conclusions in Section 5.

2. The two-fluid MHD equations

The standard one-fluid MHD approximation, extensively used to study the dynamics of plasmas in astrophysical environments, breaks down when the kinetic terms contained in the generalized Ohm's law are not negligible. Assuming a fully ionized plasma of protons and electrons and neglecting the electron's inertia, the generalized Ohm's law reduces to (Priest and Forbes, 1998)

$$\boldsymbol{E}+\frac{\boldsymbol{u}\times\boldsymbol{B}}{c}=\frac{1}{ne}\left(\frac{\boldsymbol{j}\times\boldsymbol{B}}{c}-\boldsymbol{\nabla}p_e\right)+\frac{4\pi\eta}{c^2}\boldsymbol{j}, \tag{1}$$

where n is the electron density (which is equal to the proton density because of the assumed charge quasi-neutrality), e is the electron charge, c is the speed of light, and η is the electric resistivity. The two-fluid effects are the Hall current and the electron pressure (i.e. the two first terms on the right-hand side).

The full dynamics of an incompressible plasma which includes these effects can be described by the so-called Hall-MHD equations. The Hall-MHD equations consist of the regular Navier–Stokes equation,

$$\frac{\partial\boldsymbol{U}}{\partial t}=-(\boldsymbol{U}\cdot\nabla)\boldsymbol{U}+(\boldsymbol{B}\cdot\nabla)\boldsymbol{B}-\nabla\left(P+\frac{B^2}{2}\right)+\boldsymbol{F}+\frac{1}{R}\nabla^2\boldsymbol{U} \tag{2}$$

and the modified induction equation

$$\frac{\partial\boldsymbol{A}}{\partial t}=(\boldsymbol{U}-\varepsilon\nabla\times\boldsymbol{B})\times\boldsymbol{B}+\varepsilon\nabla p_e+\frac{1}{S}\nabla^2\boldsymbol{A}. \tag{3}$$

We also assume incompressibility

$$\boldsymbol{\nabla}\cdot\boldsymbol{U}=0 \tag{4}$$

and adopt the gauge

$$\boldsymbol{\nabla}\cdot\boldsymbol{A}=0 \tag{5}$$

for the vector potential $\boldsymbol{A}$.

Eqs. (2)–(5) are the complete set of dimensionless equations, which we integrate numerically (see Section 4). The velocity $\boldsymbol{U}$ and the magnetic field $\boldsymbol{B}$ are expressed in units of a characteristic speed U_0 (we choose U_0 equal to the Alfven speed) and ε measures the relative strength of the Hall effect. The coefficient ε is defined as

$$\varepsilon=L_{\mathrm{Hall}}/L_0, \tag{6}$$

where L_0 is a characteristic length scale (the size of the box in our simulations is 2π). The Hall length $L_{\mathrm{Hall}}=c/\omega_{pi}$ is the so-called ion skin depth. R in Eq. (2) is the kinetic Reynolds number, defined as

$$R=\frac{U_0L_0}{\nu}, \tag{7}$$

where ν is the kinematic viscosity of the fluid, and S in Eq. (3) is the magnetic Reynolds number,

$$S=\frac{U_0L_0}{\eta}, \tag{8}$$

where η is the magnetic diffusivity.

In Section 4 we numerically integrate the curl of Eqs. (2)–(3). The total pressure p and the electron pressure p_e are self-consistently obtained in term of the fields $\boldsymbol{U}$ and $\boldsymbol{B}$, from the divergence of Eqs. (2)–(3) and enforcing the conditions given by Eqs. (4)–(5).

3. MHD turbulence and turbulent dynamos

Astrophysical and space plasma flows are characterized by Reynolds numbers much larger than unity, with typical values as large as $R\sim R_m\sim 10^{10-12}$. These flows are therefore likely to be in a strongly turbulent regime. The theoretical framework for the study of turbulence was first developed for non-magnetic fluids, thanks to the pioneering work of Kolmogorov (1941). Notwithstanding, the following general description applies to either hydrodynamic or MHD turbulent regimes.

In large Reynolds number flows, energy is an approximately conserved quantity. The nonlinear terms play an essential role, which is to stochastically redistribute energy fluctuations from one wavenumber to another. Only those excitations at sufficiently large wavenumbers decay by dissipative effects. As a result, this nonlinear redistribution continuously replenishes the energy being drained at the large wavenumber region (Montgomery, 1983). An increase in Reynolds number only raises the value of the wavenumbers where the dissipation takes over, but does not inhibit this net energy flow in Fourier space. According to this scenario,

three regions in Fourier space can be identified, each of them displaying a different behavior:

1 *Energy-containing region*: comprises those modes that are being excited directly by an external driver, which is usually located at small wavenumbers.
2 *Dissipation region*: corresponds to those modes where fluctuations are being efficiently quenched by dissipative (viscous or resistive) effects, located at the largest wavenumbers.
3 *Energy inertial region*: where external forces and dissipation are both negligible and only nonlinearities play a role, transferring fluctuations from one mode to another, while keeping the total energy constant.

Kolmogorov (1941), following essentially dimensional arguments, has shown that when a three dimensional incompressible fluid is submitted to external forcing with a narrow spectrum, a direct energy cascade is generated and a stationary energy spectrum is achieved, displaying the well known Kolmogorov spectrum

$$E_k = C_K \varepsilon^{2/3} k^{-5/3} \tag{9}$$

in the energy inertial region, where C_K is the Kolmogorov constant and ε is the energy dissipation rate. Kolmogorov's ideas, mainly based on scaling properties of the ideal equations and on the existence of a net energy flow through the corresponding inertial range, are usually known as *cascade theory* and have been applied to a number of turbulent systems including two and three-dimensional MHD turbulence (Montgomery, 1983). The power spectra predicted by cascade theory for the energy inertial range have in many cases been confirmed by experiments and numerical simulations.

As we have seen, the approximate conservation of energy in turbulent flows plays a decisive role in our understanding of stationary turbulent regimes. The Hall-MHD system has three ideal quadratic invariants, the total energy (i.e. kinetic plus magnetic),

$$E = \frac{1}{2}\int (U^2 + B^2)\,\mathrm{d}V, \tag{10}$$

the magnetic helicity,

$$H = \frac{1}{2}\int \boldsymbol{A}\cdot\boldsymbol{B}\,\mathrm{d}V, \tag{11}$$

and the generalized cross-helicity,

$$K = \frac{1}{2}\int (\boldsymbol{B} + \varepsilon\boldsymbol{\omega})\cdot(\boldsymbol{A} + \varepsilon\boldsymbol{U})\,\mathrm{d}V. \tag{12}$$

In MHD turbulence (i.e. ignoring two-fluid effects), the energy follows a cascade toward the microscale (just as for hydrodynamic turbulence), and the magnetic helicity follows an inverse cascade to the smallest wavenumbers of the system (Biskamp, 1993). This inverse cascade of magnetic helicity is associated with the self-organization of turbulent MHD flows, since the spatial patterns of the magnetic field are seen to progressively shift toward larger scales.

Recent high-resolution MHD simulations (see for instance Haugen et al., 2003, and also our Section 4) show that the energy power spectrum for stationary MHD turbulence in its energy inertial range is also consistent with the Kolmogorov law given in Eq. (9). In the next section we show that this behavior is maintained when the Hall effect is considered, i.e. Hall-MHD turbulence also displays a Kolmogorov energy power spectrum. This is one of the main results obtained by these numerical simulations. We also observe the signature of an inverse helicity cascade. Even though we do not have enough spatial resolution to quantitatively study this inverse cascade, we clearly observe the accumulation of magnetic helicity at the largest scales of the system, both in pure MHD and Hall-MHD simulations.

4. Numerical simulations

4.1. Description of the code

We developed a parallel pseudospectral code (see details in Mininni et al., 2003b), which was ran in a Beowulf cluster using the MPI library (i.e. *Message Passing Interface*). We integrated the Hall-MHD equations (2)–(3) in a cubic box with periodic boundary conditions and applying a $\frac{2}{3}$-rule dealiasing. The equations were evolved in time using a second order Runge–Kutta method. The total pressure $P + B^2/2$ was computed in a self-consistent fashion at each time step to ensure the incompressibility condition $\nabla\cdot\boldsymbol{U} = 0$ (Canuto et al., 1988). Similarly, the electron pressure p_e was computed consistently with the gauge condition $\nabla\cdot\boldsymbol{A} = 0$.

We present results from different runs with 128^3 spatial grid points and $\eta = \nu = 0.02$. The kinetic and magnetic Reynolds numbers for these simulations was $R = S \approx 300$. Simulations begin by subjecting the Navier–Stokes equation to a stationary helical force $\boldsymbol{F}$ (given by eigenfunctions of the curl operator) operating at a macroscopic scale $k_{\mathrm{force}} = 3$ (Mininni et al., 2003b) to reach a hydrodynamic turbulent steady state. The resulting statistically steady state is characterized by a positive kinetic helicity. The kinetic helicity is defined as $H_k = \frac{1}{2}\int \boldsymbol{U}\cdot\boldsymbol{\omega}\,\mathrm{d}V$, and is known to play a significant role in generating magnetic fields through the so-called *alpha* effect (Krause and Rädler, 1980).

4.2. MHD dynamos

Once the hydrodynamic stage of the simulation reaches a steady state, a non-helical and very weak

magnetic seed was introduced. This initial magnetic seed was generated by a δ-correlated vector potential centered at $k_{\text{seed}} = 35$. The run was continued with the same external helical force in the Navier–Stokes equation, to study the growth of magnetic energy due to dynamo action. The kinetic and magnetic dissipation length scales were properly resolved in the computational domain, i.e. we made sure that the dissipation wavenumbers remain smaller than the maximum wavenumber allowed by the dealiasing step, namely $k_{\max} = 128/3 \approx 43$.

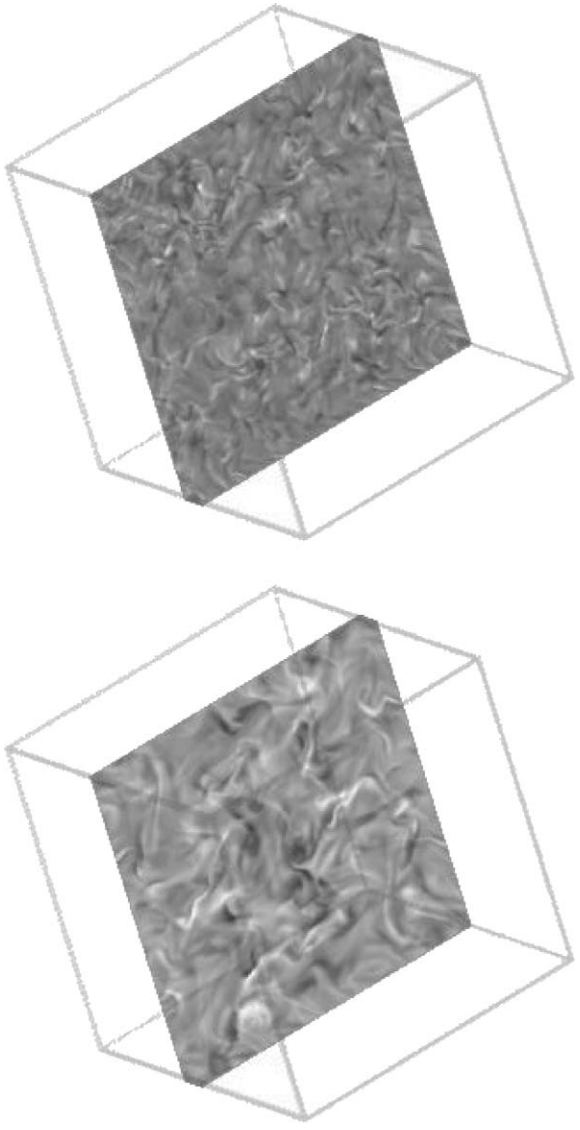

Fig. 1. Slice of a 256^3 MHD simulation displaying the component of magnetic field perpendicular to the slice. Above: right after inserting the magnetic seed. Below: when the stationary regime is reached.

Fig. 1(a) shows the spatial distribution of one of the components of the magnetic field right after the seed has been implanted, for a purely MHD run with 256^3 grid points. Fig. 1(b) shows the shift toward much larger spatial scales by about the time when the dynamo reaches saturation. Both the exponentially fast growth of magnetic energy and its net flow toward larger spatial scales are the essential ingredients for a turbulent dynamo. Within this context, turbulent dynamos can be defined as those turbulent microscale flows with the ability to generate large-scale magnetic fields.

Fig. 2 shows the kinetic and magnetic spectra at different times for a purely MHD simulation ($\varepsilon = 0$). The dotted curve at the lower right corresponds to the spectrum of the magnetic seed. During the initial kinematic stage, the magnetic energy grows uniformly at all wave numbers. After the saturation ($t \approx 5$) the emergence of a large-scale field can be clearly seen in the spectrum. At $t \approx 18.4$, when the system has already reached equipartition, the magnetic energy at large scales (small wave numbers) still remains growing slowly. As a result, the large scale magnetic field reaches super-equipartition with the kinetic energy. An excess of magnetic energy can be also observed at small scales.

As mentioned in the previous section, the slope of the total (magnetic plus kinetic) energy spectrum in the inertial range is consistent with Kolmogorov's law (Eq. (9)) and in good agreement with simulations of helical MHD turbulence with higher spatial resolution (Haugen et al., 2003).

To assess the tendency of the magnetic helicity to follow an inverse cascade, we performed simulations with the forcing wavenumber placed at $k_{\text{force}} = 10$, so that there is room for an inverse cascade to proceed. Fig. 3 shows the energy spectra taken at different times

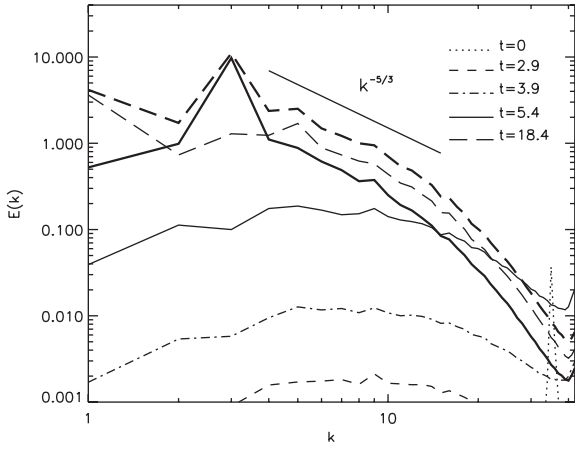

Fig. 2. Mean kinetic energy spectrum (thick line), total energy spectrum (thick dashed line), and magnetic energy spectrum at different times ($\varepsilon = 0$ and $R = 300$). The Kolmogorov's slope is shown as a reference.

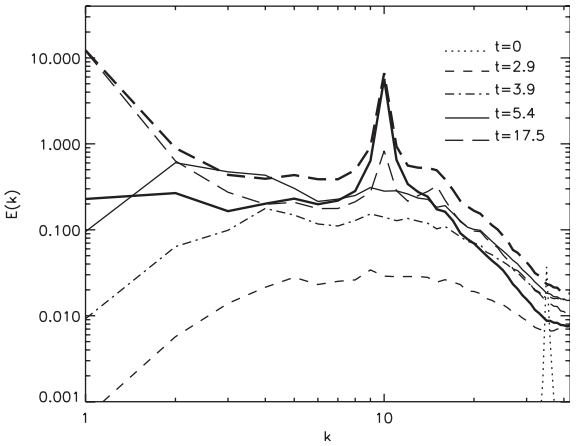

Fig. 3. Mean kinetic energy spectrum (thick line), total energy spectrum (thick dashed line), and magnetic energy spectrum at different times ($\varepsilon = 0$ and $k_{\rm force} = 10$).

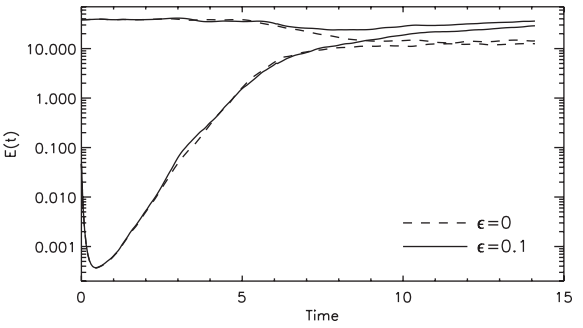

Fig. 4. Magnetic (below) and kinetic energy (above) as a function of time for two runs with $\varepsilon = 0.1$ and $\varepsilon = 0$ ($R = 300$).

for a purely MHD run, just as in Fig. 4, but with a larger value of $k_{\rm force}$. At sufficiently long times, we can clearly see the accumulation of magnetic energy at the largest scales of the system (i.e. $k = 1$). As mentioned in the previous section, this inverse cascade reflects in the progressive simplification of the magnetic spatial patterns of the system.

4.3. Hall-MHD dynamos

The Hall effect is expected to affect the MHD results on the generation of magnetic fields by inductive motions in a conducting fluid (dynamo effect). More specifically, it is expected to modify the growth and evolution of magnetic energy, since the addition of the Hall term to the MHD equations leads to the freezing of the magnetic field to the electron flow (in the non-dissipative limit) rather than to the bulk velocity field. Although the Hall effect might not be relevant for the solar dynamo, it is likely to play a significant role in other astrophysical objects, such as accretion disks (Sano and Stone, 2002). In a previous paper (Mininni et al., 2003b), we showed that three distinct dynamo regimes can be tentatively identified: (1) Hall-enhanced, (2) Hall-suppressed, (3) MHD. These regimes arise as a result of the relative ordering between the relevant lengthscales of the problem. Namely, the energy-containing scale of the flow, the Hall length, and the correlation length of the magnetic seed. The direct simulations presented here, performed at higher spatial resolution and larger Reynolds numbers, fully confirm this preliminary result. We also study the spectral distribution of the generated magnetic fields and compare with results arising from pure MHD simulations.

The simulation shown in Fig. 1 corresponds to pure MHD, i.e. it does not consider two-fluid effects. Fig. 4 shows the kinetic and magnetic energy as a function of time both for an MHD (i.e. $\varepsilon = 0$) and also for a Hall-MHD run with $\varepsilon = 0.1$ and $R = 300$.

For any given value of ε we can define a wavenumber $k_{\rm Hall} = 1/\varepsilon$. All wavenumbers smaller than $k_{\rm Hall}$ are expected to be strongly affected by the Hall current. This choice of $\varepsilon = 0.1$ (and therefore $k_{\rm Hall} = 10$) corresponds to the *Hall-enhanced* regime, as defined in Mininni et al. (2003b).

At early times, the evolution of magnetic energy in MHD and Hall-MHD is rather similar, suggesting that the Hall effect does not play much of a role during the initial stages of the dynamo. This stage corresponds to the so-called kinematic dynamo, during which: (1) the magnetic field grows exponentially fast, being advected by the strong velocity field $\boldsymbol{U}$, (2) the flow evolves essentially unaffected by the relatively weak magnetic field. The kinematic regime breaks down when the magnetic energy becomes non-negligible in comparison to the kinetic energy. Both runs are eventually seen to settle down at a saturation level characterized by the approximate equipartition between kinetic and magnetic energy. However, in Fig. 4 we can also observe that when the Hall term is included, the stationary level of magnetic (and kinetic) energy is comparatively larger.

Fig. 5 shows the kinetic, magnetic, and total energy spectra at different times for a Hall-MHD run with $\varepsilon = 0.1$. Except for ε, all the parameters and initial conditions in this run are the same as those corresponding to Fig. 2. Therefore, a direct comparison between the evolution of both spectra can be made. During the kinematic stage, the evolution is similar to the MHD run, with the entire magnetic spectrum growing at almost the same rate. The difference observed in Mininni et al. (2003b), that the large-scale magnetic field is slightly larger than in its MHD counterpart, is now increased as a result of the larger Reynolds number and larger scale separation.

Note that while the MHD spectrum shows super-equipartition at small scales (the magnetic energy is

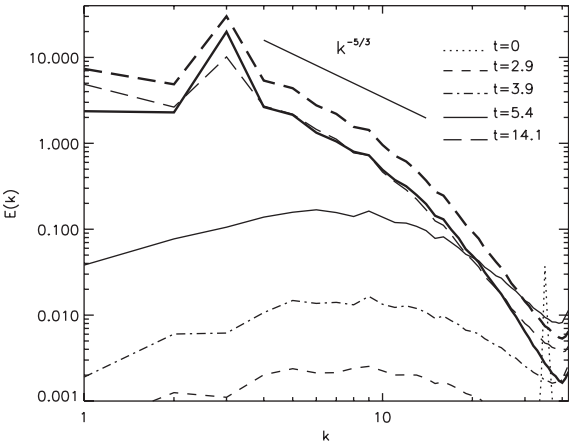

Fig. 5. Mean kinetic energy spectrum (thick line), total energy spectrum (thick dashed line), and magnetic energy spectrum at different times ($\varepsilon = 0.1$ and $R = 300$).

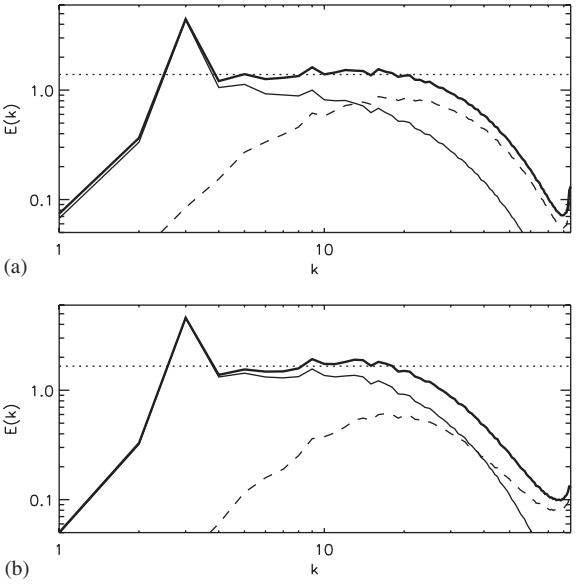

Fig. 6. Total compensated energy spectrum $k^{5/3}\varepsilon^{-2/3}E_k$ (thick line), kinetic energy spectrum (thin line), and magnetic energy spectrum (dashed line) at $t = 5.5$ for a run with (a) $\varepsilon = 0$, and (b) $\varepsilon = 0.1$.

larger than the kinetic energy at large wave numbers), the Hall-MHD leads to equipartition at these scales. Nonetheless, the total energy spectrum also follows a Kolmogorov slope, just as for the MHD case.

To quantitatively estimate the slope of the spectra, and also to obtain the corresponding Kolmogorov's constants, in Fig. 6 we display compensated power spectra, i.e. we plot $k^{5/3}\varepsilon^{-2/3}E_k$ as a function of k. Fig. 6(a) corresponds to the MHD limit (i.e. $\varepsilon = 0$), while Fig. 6(b) has $k_{\mathrm{Hall}} = 10$ ($\varepsilon = 0.1$). Both spectra have been computed at $t = 5.5$, which approximately corresponds to the nonlinear saturation of the dynamo. The parameter ε is the time average (during the stationary regime) of the energy dissipated by viscosity and electric resistivity per unit time. In a turbulent stationary regime, this time-averaged dissipation rate is approximately equal to $\int \boldsymbol{F}\cdot\boldsymbol{U}\,\mathrm{d}V$, which is the power delivered by the external force $\boldsymbol{F}$ to the flow (see Eq. (2)). During the stage of purely hydrodynamic turbulence (i.e. before the magnetic seed is introduced) we obtained a dissipation rate $\varepsilon \approx 38$. When the dynamo reaches saturation, the dissipation rate for the MHD case (i.e. $\varepsilon = 0$) settles at $\varepsilon \approx 28$, and for the Hall dynamo ($\varepsilon = 0.1$) it approximately remains at $\varepsilon \approx 38$. The slight reduction in the dissipation rate for the MHD case is consistent with a similar reduction of the r.m.s. value of the velocity field at the scale where the external force operates. This reduction becomes apparent by comparing the peaks of the kinetic energy spectra in Figs. 2 and 5.

The flat portion of the total energy spectra in Fig. 6 indicates the energy inertial range, and the height of the plateau provides the value of the corresponding Kolmogorov constant C_{K}. For the purely MHD case, the Kolmogorov constant is $C_{\mathrm{K}} \approx 1.39$, in close agreement with other simulations performed at higher spatial resolution (Haugen et al., 2003). For the Hall-MHD case, the Kolmogorov constant is $C_{\mathrm{K}} \approx 1.66$, i.e. slightly larger than its MHD counterpart. An excess of magnetic energy can be observed at small scales in Fig. 6(a), which corresponds to the MHD limit (i.e. $\varepsilon = 0$). It is interesting to note that a similar feature has been reported by Bruno et al. (1985) (see also Marsch and Tu, 1990) in connection to solar wind Alfvenic fluctuations performed by the Helios spacecraft. This excess of magnetic energy seems to vanish when the Hall effect

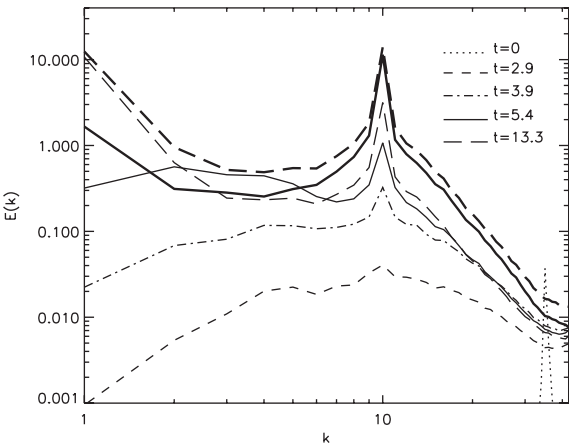

Fig. 7. Mean kinetic energy spectrum (thick line), total energy spectrum (thick dashed line), and magnetic energy spectrum at different times ($\varepsilon = 0.1$ and $k_{\mathrm{force}} = 10$).

becomes non-negligible, with the kinetic and magnetic spectra closer to an equipartition regime, as shown in Fig. 6(b).

In Fig. 7 we also show similar signatures of an inverse cascade, but for a Hall-MHD run with $\varepsilon = 0.1$ and $k_{\text{force}} = 10$. Note, however, that the kinetic energy (thick trace) at large scales ($k \approx 1$) is about one order of magnitude larger than in the MHD case. Even though the Hall effect is expected to have a strong influence on wavenumbers larger than $k_{\text{Hall}} = 10$, its effect is also apparent at smaller wavenumbers as well.

5. Conclusions

In the present paper we quantitatively study the ability of turbulent microscale plasma flows to generate large-scale magnetic fields, i.e. the efficiency of turbulent dynamos. In particular, we assess the potential relevance of the Hall effect, which is known to be non-negligible in a number of plasma flows of astrophysical interest.

We present results of direct numerical simulations of turbulent dynamo action both in pure MHD (one-fluid MHD) and Hall-MHD (two-fluid MHD). We find that the Hall-MHD dynamo works more efficiently when the Hall length is somewhat larger than the dissipation scale. This result is consistent with the scenario of the so-called Hall-enhanced regime, as reported elsewhere (Mininni et al., 2003b), from simulations at smaller spatial resolution.

Both for pure MHD and Hall-MHD, the dynamo is observed to saturate at a level of approximate equipartition between magnetic and kinetic energy, after an initial stage during which the magnetic energy grows exponentially fast. The total energy spectrum in both cases reaches the Kolmogorov power spectrum. For the case of MHD turbulence, this result is consistent with previous estimates, but to our knowledge this is the first time that the energy spectrum is derived for Hall-MHD turbulence.

We also observe the tendency of the magnetic helicity to follow an inverse cascade, with the ensuing accumulation of magnetic structure at the largest spatial scales of the system. For the Hall-MHD case, we also observe a non-negligible amount of kinetic energy being transferred to large scales, indicating that the macroscopic features of Hall-MHD flows might differ from those predicted by the one-fluid MHD approximation. These global features observed in turbulent MHD dynamos are expected to provide a basis for a microscopic theory of the *alpha* effect, which is essential for a better understanding of large scale dynamos.

Acknowledgements

The authors acknowledge a careful reading and fruitful comments from Laura Morales. This work was supported by Grants UBACyT X209, CONICET PIP 2693, and PICT 03-9483 (ANPCyT). D. G. is a member of the Carrera del Investigador Científico, CONICET.

References

Balbus, S.A., Terquem, C., 2001. Linear analysis of the Hall effect in protostellar disks. Astrophysical Journal 552, 235–247.

Biskamp, D., 1993. Nonlinear Magnetohydrodynamics. Cambridge University Press, Cambridge, UK.

Bruno, R., Bavassano, B., Villante, U., 1985. Evidence for long period Alfvn waves in the inner solar system. Journal of Geophysical Research 90, 4373–4377.

Canuto, C., Hussaini, M.Y., Quarteroni, A., Zang, T.A., 1988. Spectral Methods in Fluid Dynamics. Springer, Berlin.

Childress, S., Gilbert, A.G., 1995. Stretch, Twist, Fold: The Fast Dynamo. Springer, Berlin.

Deng, X.H., Matsumoto, H., 2001. Rapid magnetic reconnection in the Earth's magnetosphere mediated by whistler waves. Nature 410, 557–560.

Haugen, N.E.L., Brandenburg, A., Dobler, W., 2003. Is nonhelical hydromagnetic turbulence peaked at small scales? Astrophysical Journal 597, L141–L144.

Kolmogorov, A.N., 1941. Dissipation of energy in a locally isotropic turbulence. Doklady Akad. Nauk SSSR 32, 141 (in Russian).

Krause, F., Rädler, K.-H., 1980. Mean-Field Magnetohydrodynamics and Dynamo Theory. Pergamon Press, GDR.

Marsch, E., Tu, C.-Y., 1990. On the radial evolution of MHD turbulence in the inner heliosphere. Journal of Geophysical Research 95, 8211–8229.

Mininni, P.D., Gómez, D.O., Mahajan, S.M., 2002. Dynamo action in Hall magnetohydrodynamics. Astrophysical Journal 567, L81–L83.

Mininni, P.D., Gómez, D.O., Mahajan, S.M., 2003a. Role of the Hall current in MHD dynamos. Astrophysical Journal 584, 1120–1126.

Mininni, P.D., Gómez, D.O., Mahajan, S.M., 2003b. Dynamo action in MHD and Hall-MHD. Astrophysical Journal 587, 472–481.

Montgomery, D., 1983. Theory of hydromagnetic turbulence. In: Neugebauer, M. (Ed.), Solar Wind V. NASA Conf. Publ., 2280, p. 107.

Morales, L., Dasso, S., Gómez, D., Mininni, P., 2004. Hall magnetic reconnection at the Earth's magnetopause. Journal of Atmospheric and Solar Terrestrial Physics, submitted for publication.

Øieroset, M., et al., 2001. In situ detection of collisionless reconnection in the Earth's magnetotail. Nature 416 (26), 414–416.

Priest, E., Forbes, T., 1998. Magnetic Reconnection. Cambridge University Press, Cambridge.

Sano, T., Stone, J.M., 2002. The effect of the Hall term on the nonlinear evolution of the magnetorotational instability. Astrophysical Journal 570, 314–328.